Michael Krause (Autor)

Efficient Raman Amplifiers and Lasers in Optical Fibers and Silicon Waveguides: New Concepts

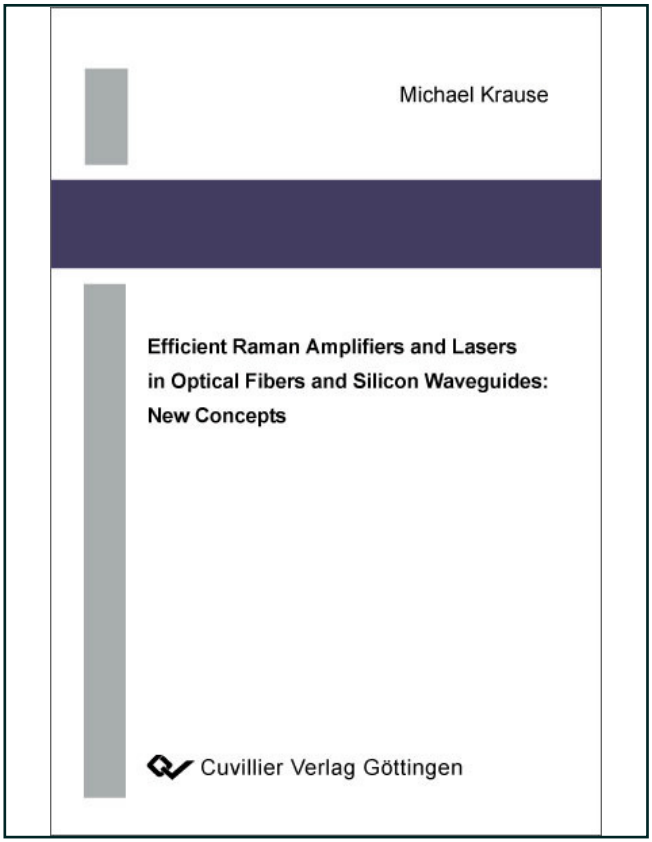

https://cuvillier.de/de/shop/publications/1796

Copyright:
Cuvillier Verlag, Inhaberin Annette Jentzsch-Cuvillier, Nonnenstieg 8, 37075 Göttingen, Germany
Telefon: +49 (0)551 54724-0, E-Mail: info@cuvillier.de, Website: https://cuvillier.de

1. Introduction

Raman amplifiers and lasers in fiber-optic communications

Optical amplifiers are key elements of any fiber-optic communication system. Even though modern optical fibers have losses below 0.2 dB/km, a repeated amplification of the transmitted signal to its original strength becomes necessary at long enough distances. One solution for signal regeneration is the conversion of the optical signal into the electrical domain and subsequent re-conversion into a fresh optical signal. However, purely optical amplifiers are usually preferred. They simply amplify the electromagnetic field of the signal via stimulated emission or stimulated-scattering processes in a certain optical frequency range. The amplification process is essentially independent of the details of the spectral channel layout, modulation format or data rate of the transmission span, thus permitting the system operator to later re-configure these parameters without having to upgrade the amplifiers.

For a distributed Raman fiber amplifier (RFA), power is provided by optical pumping of the transmission fiber; the pump wavelength is shorter than the wavelength to be amplified by an amount that corresponds to an optical frequency difference of about 13.2 THz. The signal then experiences gain due to Stimulated Raman Scattering (SRS), a nonlinear optical process in which a pump photon is absorbed and immediately re-emitted in the form of a phonon and a signal photon, thus amplifying the signal. Fig. 1.1

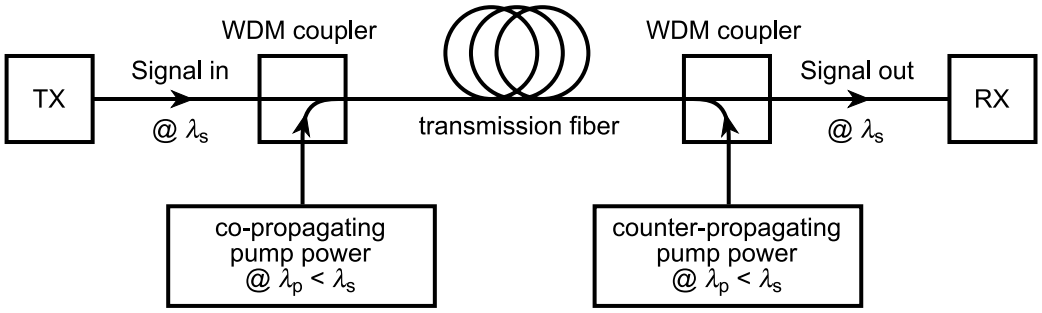

Figure 1.1.: Schematic of a Raman fiber amplifier. The pump power at wavelength λ_p, often provided by Raman fiber lasers, may be co- or counter-propagating (or both) with the signal to be amplified at λ_s.

shows a schematic view of a Raman-amplifed transmission link [1, 2].

RFAs had been investigated already in the 1980s, but the relatively large required pump powers were not conveniently available at that time, so that RFAs were deemed impractical. During the 1990s, the erbium-doped fiber amplifier (EDFA) was the favored and well-established practical alternative. With the advent of high-power semiconductor lasers, however, the RFA could finally be considered for employment in practical transmission systems. This was desirable because RFAs have several advantages over EDFAs, such as better noise performance and increased spectral flexibility—in fact, Raman amplification is possible throughout the entire transparency range of fibers (provided suitable 13.2-THz-shifted pump sources are available), while EDFAs are limited by the emission spectrum of the erbium ions. By 2000, communications equipment incorporating Raman technology was commercially available.

Soon after that, in 2003, Jalali's group at the University of California in Los Angeles could demonstrate a Raman amplifier in a silicon waveguide. While in optical fibers lengths of several hundreds of meters are required to achieve significant Raman gain, in silicon a waveguide of several centimeters is sufficient because of the much larger Raman-gain coefficient of silicon. This being the first time that an optical amplifier could be demonstrated in silicon, the result marked a milestone in the development of the field of silicon-based photonics, which has recently seen significant progress in other areas as well. Today, silicon photonics can provide most of the functionality required for integrated optics [3, 4].

Silicon-based optical-communications components are so widely researched because they have the potential of being mass-produced at low cost, by making use of the existing infrastructure of the electronics industry. A high demand for such components may arise in environments where low cost is more important than ultimate performance, such as in the context of emerging optical access networks. On-chip Raman amplifiers could compensate for silicon-waveguide losses and make possible the realization of complex passive photonic circuitry in a compact form [4].

Finally, the pump sources for RFAs are often Raman fiber lasers (RFLs), which make use of the stimulated Raman effect just like the amplifier itself. RFLs, too, have been researched since the 1980s [1, 2]. In silicon, on the other hand, the first continuous-wave Raman laser was demonstrated only very recently, in 2005, by Paniccia's research group at Intel Corporation, thus setting yet another silicon-photonics milestone.

Thus, with Raman fiber amplifiers and lasers already well-established in state-of-the-art long-haul transmission links, Raman-based silicon components may one day be a key element of low-cost fiber-optic communications equipment, too.

Overview of this thesis

The aim of this thesis was to develop, model and optimize novel concepts for Raman amplifiers and lasers both in fibers and silicon waveguides that have the potential of improving the performance of fiber-optic communication systems.

The starting chapter 2 derives the equations required for the modeling of Raman amplifers and lasers in optical waveguides, especially in fibers. The following two chapters present new designs for Raman fiber lasers: while chapter 3 concentrates on their power efficiency and spectral flexibility, chapter 4 investigates stability properties of RFLs.

Chapter 5 prepares for the second part of the thesis by summarizing the material properties of silicon and extending the RFL model to include the nonlinear absorption effects significant in silicon waveguides. In chapter 6, fundamental properties of silicon Raman amplifiers are derived and several new designs of amplifiers with improved characteristics are proposed. The last chapter 7 analyzes the basic behavior of silicon Raman lasers and finally proposes new designs with increased efficiency. Chapter 8 concludes the thesis.

Details about the mode-solving software that was written for the simulations in chapters 6 and 7 are given in the appendix, followed by a list of the author's publications and the references.

References

[1] M. N. Islam, editor. *Raman Amplifiers for Telecommunications 1 & 2.* Springer-Verlag, 2004.

[2] C. Headley and G. P. Agrawal, editors. *Raman Amplification in Fiber Optical Communication Systems.* Elsevier, 2005.

[3] L. Pavesi and G. Guillot, editors. *Optical Interconnects – The Silicon Approach.* Springer-Verlag, 2006.

[4] B. Jalali, M. Paniccia and G. Reed. Silicon Photonics. *IEEE Microwave Magazine*, 7(3):58–68, June 2006.

2. Stimulated Raman scattering in optical waveguides

This introductory chapter forms the foundation for the remainder of this thesis. Section 2.1 gives an introduction to the Raman effect, which all of the devices analyzed in this thesis are based on. Section 2.2 derives the nonlinear Schrödinger equations (NLSEs) that model the propagation of guided waves coupled by a third-order nonlinearity. Finally, section 2.3 specializes the model to the case of Raman amplification in optical fibers, thus preparing for chapters 3 and 4.

2.1. The Raman effect

Spontaneous Raman scattering is a nonlinear optical process in which a photon, called the "pump" photon, is absorbed by a material while simultaneously a photon of a different energy is emitted. The difference in photon energy is compensated by a change of the vibrational state of the material [Sto04].

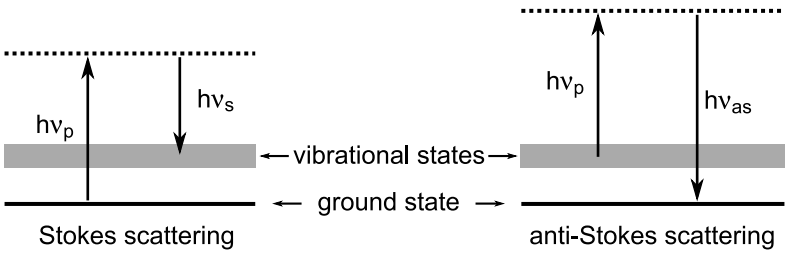

Figure 2.1.: Illustration of spontaneous Stokes and anti-Stokes Raman scattering.

Fig. 2.1 illustrates the two basic types of spontaneous Raman scattering. In so-called Stokes scattering (Fig. 2.1a), a pump photon of energy $h\nu_p$ is absorbed, and a Stokes photon of energy $h\nu_s < h\nu_p$ is emitted, while the material undergoes a transition to a higher vibrational energy state. On the other hand, Anti-Stokes scattering can occur when the material already is in an excited vibrational state. Then, a pump photon of energy $h\nu_p$ is absorbed, and a quantum of vibrational energy is added to that energy to

yield an anti-Stokes photon of higher energy $h\nu_{as} > h\nu_p$, see Fig. 2.1b. The anti-Stokes process is much weaker than the Stokes process, so it is usually neglected in the modeling of Raman amplifiers and lasers [Agr01, HA05].

Stimulated Raman scattering (SRS) occurs when photons at the Stokes wavelength are already present in addition to the pump photons, e. g., when deliberately injecting both a pump and a Stokes beam into the material. Then the rate of the Stokes processes illustrated in Fig. 2.1a is increased: the more Stokes photons are already present, the faster additional Stokes photons are added. In other words, the Stokes beam is amplified [Sto04]. The evolution of the Stokes intensity I_s along the propagation direction z due to SRS can be written in the form

$$\frac{\mathrm{d}I_s}{\mathrm{d}z} = g_R I_p I_s, \tag{2.1}$$

where I_p is the pump intensity—the Raman gain per unit length experienced by the Stokes wave is proportional to the pump intensity and to the Raman-gain constant g_R, which is a property of the nonlinear material. In many cases of practical interest, the Stokes powers are large enough such that SRS dominates and the small effect of spontaneous Raman scattering can be neglected as in Eq. (2.1). SRS can then be described mathematically as a third-order nonlinear effect in terms of a nonlinear susceptibility $\chi^{(3)}$, see section 2.2.

Finally, the Raman-gain constant depends on the optical frequency difference between the pump and Stokes beams. As Fig. 2.1 shows, significant Stokes scattering and thus SRS gain is only obtained when the pump-Stokes frequency difference corresponds to the energy of a vibrational excitation of the material. On the one hand, in crystalline materials such as silicon the vibrational energies are very well defined; the Raman-gain maximum in silicon occurs at a frequency which is 15.6 THz below that of the pump beam, and the gain linewidth is about 100 GHz, see section 5.2.1. On the other hand, in optical fibers based on fused silica the vibrational energy levels are spread over a broad range of frequencies due to the amorphous structure of the material. Here, the gain maximum occurs at a frequency shift of 13.2 THz, but the gain is significant over a range of 6 THz, see Fig. 2.3 on page 20. The effective width of the gain spectrum can even be increased further by pumping Raman fiber amplifiers with several closely spaced pump wavelengths [HA05].

2.2. Mathematical model of nonlinear wave coupling

The models describing amplifiers and lasers in this thesis are based on the formalism of coupled nonlinear Schrödinger equations (NLSEs), which are differential equations

describing the evolution of spatially and temporally varying field envelopes of optical beams propagating inside the waveguide, which are coupled through the waveguide nonlinearity. The absolute square of these field envelopes gives the instantaneous powers of the various beams, which are the quantities of primary interest in the discussions in later chapters.

In this section, the derivation of the NLSEs from Maxwell's equations will be sketched. For clarity, we restrict ourselves to the special case of a waveguide inside which forward- and backward-propagating beams at only two center wavelengths are propagating. Many types of Raman amplifiers and lasers can be successfully described by such a model, where the two wavelengths correspond to the pump and Stokes wavelengths. Eqs. (2.38) and (2.39) will be the main results of this section.

The derivation of the coupled NLSEs sketched in sections 2.2.1–2.2.4 basically follows that of [SdSE02], although we treat the nonlinear polarization in the frequency domain as in [PV86] and we consider the specific case of both co- and counterpropagating beams at two center frequencies.

An extension of this model to the case of more than two wavelengths is straightforward, however, and will be briefly summarized at the appropriate points in later chapters. Also, we will not deal with the effect of Free-Carrier Absorption here—for this we need to take into account the optical generation of charge carriers and their influence on the light propagating inside the waveguide; this effect will be incorporated in the model in Sect. 5.4.

2.2.1. Overview

We consider a longitudinally invariant waveguide, such as an optical fiber (for chapters 3 and 4) or a silicon waveguide (for chapters 6 and 7). Light is coupled into the waveguide the intensity of which is so strong that there will be a significant nonlinear material response influencing the light propagation. The evolution of the electromagnetic field is described by Maxwell's equations,

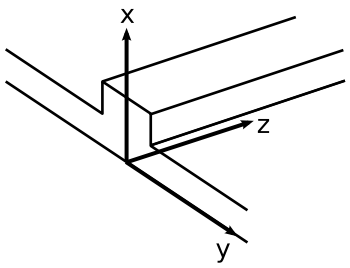

Figure 2.2.: Coordinate system used throughout this thesis. The waveguide is oriented along the z axis.

$$\nabla \times \tilde{\mathbf{E}} = -\mu_0 \frac{\partial \tilde{\mathbf{H}}}{\partial t}, \qquad \nabla \times \tilde{\mathbf{H}} = \frac{\partial}{\partial t}(\epsilon_0 n^2 \tilde{\mathbf{E}} + \tilde{\mathbf{P}}) + \tilde{\mathbf{J}}, \tag{2.2}$$

$$\nabla \cdot (\epsilon_0 n^2 \tilde{\mathbf{E}} + \tilde{\mathbf{P}}) = \tilde{\rho}, \qquad \nabla \cdot \tilde{\mathbf{H}} = 0 \tag{2.3}$$

for the electric and magnetic fields $\tilde{\mathbf{E}}(\mathbf{r},t)$ and $\tilde{\mathbf{H}}(\mathbf{r},t)$, where $\mathbf{r}=(x,y,z)$ is a vector, and the tilde denotes a time-domain function. Fig. 2.2 shows the coordinate system used here. The fields are prescribed over certain surfaces, e. g., at one end of the waveguide, where optical power is coupled in, and we want to know how the fields evolve inside the waveguide.

In this chapter, we assume that there are no free carriers in the waveguide, such that the charge and current densities are zero, $\tilde{\rho}=0$ and $\tilde{\mathbf{J}}=0$. Later in chapter 5, the effect of Free-Carrier Absorption will be included, which will be treated only for the CW case and in the ambipolar approximation, i. e., the excess hole and electron densities are equal at each point such that again $\tilde{\rho}=0$, and there is no net electric current ($\tilde{\mathbf{J}}=0$), see section 5.4.1. We will therefore assume $\tilde{\rho}=0$ and $\tilde{\mathbf{J}}=0$ throughout this thesis.

The refractive-index profile $n(x,y)$ of the waveguide does not vary along the waveguide axis z. The polarization $\tilde{\mathbf{P}}(\mathbf{r},t)$ represents the nonlinear response of the material. The materials considered here (amorphous fused silica or crystalline silicon) have no significant second-order nonlinearity due to their centrosymmetry [Agr01, Boy03]. We therefore consider third-order nonlinearities of the form [Boy03, Mil98]

$$\tilde{P}^i(\mathbf{r},t)=\epsilon_0\iiint_0^\infty \tilde{\chi}^{(3)}_{ijkl}(\tau_1,\tau_2,\tau_3)\tilde{E}^j(\mathbf{r},t-\tau_1)\tilde{E}^k(\mathbf{r},t-\tau_2)\tilde{E}^l(\mathbf{r},t-\tau_3)\,\mathrm{d}\tau_1\,\mathrm{d}\tau_2\,\mathrm{d}\tau_3, \quad (2.4)$$

where the superscripts $i,j,k,l=x,y,z$ denote cartesian field components, and we have used the Einstein notation for writing the products involving the fields and the nonlinear susceptibility tensor $\tilde{\chi}^{(3)}_{ijkl}$, i. e., a summation over $j,k,l=x,y,z$ is implicit on the right-hand side. The third-order nonlinear polarization at a time t given by Eq. (2.4) depends on the electric field at all earlier times and along all cartesian directions according to the response function $\tilde{\chi}^{(3)}_{ijkl}(\tau_1,\tau_2,\tau_3)$, which is zero for negative time lags $\tau_{1,2,3}$ due to causality. Expression (2.4) is sufficiently general that it can describe effects such as stimulated Raman scattering (SRS), two-photon absorption (TPA), self-phase modulation (SPM), cross-phase modulation (XPM), and four-wave mixing (FWM).

The coupled NLSEs, which will be derived during the rest of this chapter, are an approximate reformulation of Eqs. (2.2)–(2.4) which is easier to handle. The basic assumption is that the electromagnetic field in the waveguide can be thought of as consisting of one or only a few beams centered spectrally around specific center frequencies and propagating in specific waveguide modes. These beams will interact inside the waveguide through its nonlinearity, which can in principle result in the generation of light at any optical frequency and in any waveguide mode. However, often these new components can build up significantly only if certain phase-matching conditions are fulfilled, which is generally not the case unless the waveguide is specifically designed for that purpose.

Using the NLSE approach requires one to make a reasonable assumption about what optical frequencies and waveguide modes are significant in the problem at hand.

In the rest of this chapter we will assume that light propagates only in the vicinity of two frequencies, ω_p (pump) and ω_s (Stokes) in our waveguide. Taking into account the two propagation directions, we have four beams in total (forward- and backward-propagating waves at ω_p and ω_s, respectively). We will derive four coupled NLSEs that describe the evolution of these waves along the waveguide, see Eqs. (2.38)–(2.39). They form the basis for the description of all Raman amplifiers and laser in later chapters.

2.2.2. Modal description of light propagation

Fourier-transform conventions

Throughout this thesis, the Fourier transform of any function of time $\tilde{\Psi}(t)$, such as any cartesian component of the electric and magnetic fields $\tilde{\mathbf{E}}(\mathbf{r},t)$ and $\tilde{\mathbf{H}}(\mathbf{r},t)$, is defined according to the convention in [Fli91],

$$\Psi(\omega) = \int_{-\infty}^{+\infty} \tilde{\Psi}(t) e^{-j\omega t}\,\mathrm{d}t, \tag{2.5}$$

such that the inverse Fourier transform is given by

$$\tilde{\Psi}(t) = \frac{1}{2\pi}\int_{-\infty}^{+\infty} \Psi(\omega) e^{j\omega t}\,\mathrm{d}\omega. \tag{2.6}$$

As we are only dealing with real time signals, we have $\Psi(-\omega) = \Psi^*(\omega)$.

Fourier transformation and modal decomposition of Maxwell's equations

The first step to an approximate solution of Eqs. (2.2)–(2.3) with $\tilde{\rho} = 0$ and $\tilde{\mathbf{J}} = 0$ is a Fourier transformation, leading to Maxwell's equations in the frequency domain,

$$\nabla \times \mathbf{E} = -j\omega\mu_0\mathbf{H}, \qquad \nabla \times \mathbf{H} = j\omega(\epsilon_0 n^2\mathbf{E} + \mathbf{P}), \tag{2.7}$$

$$\nabla \cdot (\epsilon_0 n^2\mathbf{E} + \mathbf{P}) = 0, \qquad \nabla \cdot \mathbf{H} = 0, \tag{2.8}$$

The transverse fields (the x and y components) of the solution of Eqs. (2.7)–(2.8) (for any nonlinear polarization $\mathbf{P}$) can be expanded in the complete set of forward- (+) and backward-propagating (−) normal modes of the linear ($\mathbf{P} = 0$) waveguide [SL83],

$$\mathbf{E}^t(\mathbf{r},\omega) = \sum_m \left[A_m^+(z,\omega)e^{-j\beta_m(\omega)z} + A_m^-(z,\omega)e^{j\beta_m(\omega)z}\right]\mathbf{e}_m^{+,t}(x,y,\omega), \tag{2.9}$$

$$\mathbf{H}^t(\mathbf{r},\omega) = \sum_m \left[A_m^+(z,\omega)e^{-j\beta_m(\omega)z} - A_m^-(z,\omega)e^{j\beta_m(\omega)z}\right]\mathbf{h}_m^{+,t}(x,y,\omega), \tag{2.10}$$

where the fields $\mathbf{e}_m^+$ and $\mathbf{h}_m^+$ are the forward-propagating modes of the linear waveguide with propagation constants β_m. The superscript t denotes the transverse part of the corresponding vector, and we are using the convention that the forward- and backward-propagating mode fields are related as

$$\mathbf{e}_m^+ = \mathbf{e}_m^{+,t} + e_m^{+,z}\hat{\mathbf{z}}, \qquad \mathbf{h}_m^+ = +\mathbf{h}_m^{+,t} + h_m^{+,z}\hat{\mathbf{z}}, \tag{2.11}$$

$$\mathbf{e}_m^- = \mathbf{e}_m^{+,t} - e_m^{+,z}\hat{\mathbf{z}}, \qquad \mathbf{h}_m^- = -\mathbf{h}_m^{+,t} + h_m^{+,z}\hat{\mathbf{z}}, \tag{2.12}$$

and the transverse electric fields $\mathbf{e}_m^{\pm,t}$ are chosen real [SL83]. The summations over m in Eqs. (2.9)–(2.10) are understood to represent the summation over the finite number of guided modes and the integration over all propagating and evanescent radiation modes.

Using the conjugated reciprocity theorem [SL83, SF03], one can show that the expansion coefficients $A_m^\pm(z,\omega)$ occuring in Eqs. (2.9)–(2.10) are related to the perturbing polarization $\mathbf{P}(\mathbf{r},\omega)$ through the coupled-mode equations[1]

$$\frac{\partial A_m^\pm(z,\omega)}{\partial z} = \mp j\frac{\omega}{4N_k(\omega)} e^{\pm j\beta_m(\omega)z} \int \mathbf{e}_m^{\pm *}(x,y,\omega)\cdot\mathbf{P}(x,y,z,\omega)\,\mathrm{d}A, \tag{2.13}$$

with the mode normalization

$$N_k(\omega) = \frac{1}{2}\int \left[\mathbf{e}_k^+(x,y,\omega)\times\mathbf{h}_k^{+*}(x,y,\omega)\right]\cdot\hat{\mathbf{z}}\,\mathrm{d}A. \tag{2.14}$$

The frequency-domain polarization $\mathbf{P}(\mathbf{r},\omega)$ occuring in Eq. (2.13) is obtained upon Fourier-transforming Eq. (2.4) as

$$P^i(\mathbf{r},\omega) = \frac{\epsilon_0}{4\pi^2}\iint_{-\infty}^{+\infty} \chi^{(3)}_{ijkl}(\omega_1,\omega_2,\omega-\omega_1-\omega_2) \cdot E^j(\mathbf{r},\omega_1)E^k(\mathbf{r},\omega_2)E^l(\mathbf{r},\omega-\omega_1-\omega_2)\,\mathrm{d}\omega_1\,\mathrm{d}\omega_2, \tag{2.15}$$

where the frequency-dependent $\chi^{(3)}_{ijkl}$ tensor is the Fourier-transformed response function,

$$\chi^{(3)}_{ijkl}(\omega_1,\omega_2,\omega_3) = \iiint_{-\infty}^{+\infty} \tilde{\chi}^{(3)}_{ijkl}(\tau_1,\tau_2,\tau_3)e^{-j(\omega_1\tau_1+\omega_2\tau_2+\omega_3\tau_3)}\,\mathrm{d}\tau_1\,\mathrm{d}\tau_2\,\mathrm{d}\tau_3. \tag{2.16}$$

The expression for the polarization, Eq. (2.15), explicitly shows that the nonlinearity can couple different frequency components of the field — on the other hand, in a linear waveguide all frequency components would propagate independently.

[1] Strictly speaking, Eq. (2.13) is only valid for modes with a real propagation constant β_m; the modification necessary for evanescent modes is not given here, as their contribution to our effects is so weak that we may neglect them.